J Appl Electrochem (2012) 42:145–151
DOI 10.1007/s10800-012-0381-9

ORIGINAL PAPER

Carbon nanotube-modified biocatalytic microelectrodes with multiscale porosity

Hao Wen · Harshal Manubhai Bambhania · Scott Calabrese Barton

Received: 27 September 2011 / Accepted: 20 January 2012 / Published online: 4 February 2012

Abstract Macropores were introduced into nanotube matrices via polystyrene bead templates, and the resulting matrix was applied to carbon fiber microelectrodes as a porous medium for immobilization of enzymatic biocatalysts. The macropores were found to increase the electrochemically active surface area by twofold at a nominal polystyrene mass fraction of 73%. The modified electrodes were further coated with biocatalyst hydrogel comprising glucose oxidase, redox polymer, and crosslinker to create a glucose oxidizing bioanode. Glucose oxidation current density also increased two fold after introduction of the macropores. Focused ion beam cut cross-sections reveal complete adsorption of the enzyme-hydrogel matrix into the CNT layer. This templating technique is a promising approach to the maximization of surface area and transport in bioelectrodes.

Keywords Carbon nanotubes · Carbon fiber microelectrode · Polystyrene particles · Biofuel cells · Electrocatalysis

1 Introduction

Biofuel cells are electrochemical devices that convert biofuel substrates or biomass into electricity [1]. They are suitable for mobile and distributed power applications due to their capability to carry out reactions near room temperature, neutral pH, and their selectivity toward reactants [2]. Among other techniques, immobilization of enzymes in redox hydrogels has been proved to enhance enzyme activity due to the mediator conducting effect between current collector and enzyme active centers [3, 4]. However, low-active site density and inefficient electron transfer have limited the achievable current density to $\sim$1 mA cm^{-2} for biofuel cells [5, 6].

High-surface area materials have been extensively employed to improve electrode efficiency [7, 8]. Carbon papers have been used as porous supports for bioelectrodes [9–12]. Carbon fiber microelectrodes (CFMEs) have been applied as a component for miniature biofuel cells [13, 14] and as a platform to study lithium ion intercalation in lithium ion batteries [15, 16]. Various morphologies including beveled fiber surfaces [17], single fibers isolated in carbonate grooves [13], nanoporous fibers [18], fibers with branching carbon nanotubes (CNTs) [19, 20], and exposed carbon fiber coated with porous CNTs [21] have been studied. In the latter study, suffusion of a porous CNT layer with a hydrogel containing redox mediator and glucose oxidase yielded a glucose oxidizing microelectrode with increased current density. It was shown that glucose oxidation current density was directly proportional to CNT surface area, suggesting that mass transport of glucose into the CNT layer was not rate limiting. However, it was not clear that CNT surface area was maximally utilized by the biocatalyst, because the typical 50-nm pore size of the CNT layer could inhibit absorption of the biocatalyst hydrogel precursor solution.

One approach to address this limitation is to introduce macropores into the CNT layer. Pore former techniques, in which template materials are removed either by dissolution or heat treatment to introduce arrays of macropores, are promising candidates to enhance transport in dense porous media [22]. Template materials can be formed by filtering colloidal particle dispersions [23–27], oil emulsion droplets [28, 29], or self-assembly [23, 30, 31]. Such porous

H. Wen (✉) · H. M. Bambhania · S. Calabrese Barton
Michigan State University, East Lansing, MI, USA
e-mail: wenhao@msu.edu

carbons have been widely applied for fuel cell catalyst supports [32]. For example, polystyrene spheres combined with silica particles served as a template for a bimodal-ordered porous catalyst support for direct methanol fuel cells [33]. Mano et al. [28] have used macroporous carbon foam formed on a silica template as a support for glucose oxidase bioelectrode.

In the current study, polystyrene (PS) particles were used as pore formers to introduce macropore morphology in a CNT matrix, using the CFME as a test platform. Varying volume fractions of PS were produced by controlling the PS to CNT mass ratio in a precursor suspension. PS/CNT suspensions were applied to CFMEs via pipette at controlled volumes. Heat treatment at 450 °C in air burned away the PS particles, leaving macropores within the CNT matrix. A focused ion beam (FIB) was used to cut through the fiber electrodes to reveal the cross-section of the modified carbon fibers. This technique enabled us to observe the PS and PS-derived pore distribution within the CNT matrix. The structure was further coated with enzymatic hydrogel to carry out glucose oxidation.

2 Experimental

2.1 Materials and chemicals

Carbon fibers of 7.0 ± 0.3 μm diameter were obtained from Goodfellow (Huntingdon, UK). Carboxylated multiwall carbon nanotubes were purchased from Nanocyl (NC3101, Sambreville, Belgium). Conductive carbon paint was purchased from SPI Supplies (West Chester, PA). Glass capillary was purchased from A-M Systems (Carlsborg, WA) and used as fiber electrode body material. *N*,*N*-dimethylformamide (DMF) was obtained from Fisher BioReagents (Hampton, NH). Monodispersed polystyrene micro particle suspension and glucose oxidase (GOx) from *Aspergillus niger* were purchased from Sigma-Aldrich (St. Louis, MO). The synthesis of redox polymer poly(vinylimidazole)-[Os(bipyridine)$_2$Cl]$^{+/2+}$ can be found elsewhere [3]. Poly(ethylene glycol) (400) diglycidyl ether (PEGDGE) was obtained from Polysciences (Warrington, PA). Sodium periodate was purchased from MP Biomedicals (Solon, OH). Nitrogen gas was obtained from Airgas. D-Glucose, sodium bicarbonate, sodium phosphate monobasic, and sodium phosphate dibasic were purchased from J.T. Baker (Phillipsburg, NJ) and used as received.

2.2 Sealing of carbon fiber into glass capillary

A micropipette puller (Sutter Instrument, P-30, Novato, CA) was used to fuse-seal carbon fibers into pulled glass capillary tips. The carbon fibers were connected to copper wires through conductive carbon paint at the open end of the capillary. Single fibers were thus sealed tightly with glass and aligned well with the pointing tip, enabling easy handling and electrolyte insulation from copper wires. Exposed carbon fiber length was maintained at 1 cm.

2.3 Preparation of CNT/PS suspensions and immobilization on single carbon fibers

A 1-mg mL^{-1} suspension of carboxylated carbon nanotubes in DMF was ultra-sonicated for 1 h for uniform dispersion. DMF is a polar, aprotic solvent that is miscible with water. This CNT/DMF dispersion was stable for at least a week.

The PS particles were received as a monodispersed aqueous suspension, which was added to CNT/DMF suspension to make a PS/CNT/DMF precursor suspension to be subsequently applied to the CFMEs. Particle size and PS number concentration, as given in product specifications, allowed calculation of final PS volume fractions in CNT matrix after solvent evaporation. The PS/CNT/DMF suspension was applied to the entire exposed carbon fiber length (1 cm) by brushing with a micropipette tip. The freshly coated CFMEs were rinsed with DI water and dried at 70 °C for 1 h to fully remove DMF before usage.

PS/CNT-coated CFMEs were heat treated under air for 4 h at 450 °C to remove PS particles, following a previous procedure [30]. Heat treatment for shorter times, e.g., 2 h yielded samples that exhibited high-ohmic resistance with residual gel-like PS phases observable by SEM. CFMEs heat treated for 4 h exhibited neither of these phenomena. Multiwall CNTS have been shown to be stable up to 500 °C by TGA analysis [38].

2.4 Surface morphology and thickness characterization

A scanning electron microscope (SEM, JEOL JSM-7500F, 5.0 kV accelerating voltage and 2 mm working distance) and an optical microscope (Nikon Eclipse LV150, Tokyo, Japan) were used to observe the surface morphology of CFMEs. Carbon fiber thicknesses were digitally measured by MATLAB®, averaging over a ~1.3-mm length of fiber.

Capacitive surface area was estimated by cyclic voltammetry in phosphate buffer solution (PBS, 20 mM phosphate, pH 7.0, with 0.1 M NaCl as supporting electrolyte), at 37.5 °C, with varying scanning rates from 0.4 to 0.5 V versus Ag/AgCl. This potential range was chosen to minimize background current. Non-faradaic currents were plotted against scanning rates, the slope of which was recorded as the capacitance. Surface area was estimated from capacitance using an assumed specific capacitance of 25 μF cm^{-2}, which is representative of carbon materials [34].

2.5 Cross-sectional morphology imaging

Cross-sections of single carbon fibers were cut and revealed by FIB-SEM (Carl Zeiss NTS GmbH, Germany). Bulk cutting through fibers was accomplished with a FIB of 20 nA at 30 kV. The revealed surface was subsequently polished using a small beam current of 1 nA at 30 kV. Final micrographs were collected with SEM detectors.

2.6 Biocatalyst coating

The preparation of biocatalyst precursor solution has been previously reported [9, 11]. A solution of 40 mg mL^{-1} GOx was prepared with 0.1 M $NaHCO_3$, mixed with 7 mg mL^{-1} sodium periodate at 1:2 volume ratio, and cured for 1 h in darkness [35, 36]. Final precursor solution was made by mixing 2 μL periodate-oxidized GOx, 8 μL 10 mg mL^{-1} PVI-$[Os(bipyridine)_2Cl]^{+/2+}$ redox polymer mediator, and 0.5 μL of 2.5 mg mL^{-1} PEGDGE crosslinker. CFMEs modified with 2 μg cm^{-1} CNTs were coated with 1 μL cm^{-1} of precursor solution and cured for 12 h in room temperature air before further tests. The above protocol leads to an electrode with 12 μg cm^{-1} solids loading with 59 wt% mediator, 40 wt% enzyme, and 1 wt% crosslinker.

2.7 Electrochemical characterization

Electrochemical characterization was conducted in a water-jacketed cell containing 50 mL PBS at 37.5 °C and pH 7.0, made oxygen-free by nitrogen sparging. The reference electrode was Ag/AgCl (Fisher Scientific, Hampton, NH), with a platinum wire counter electrode. Convection was introduced by rotating a magnetic stirring bar at 150 rpm. Redox polymer characterization was done with cyclic voltammetry using a VSP potentiostat (Bio-Logic, Knoxville, TN) at 50 mV s^{-1} scan rate from 0.0 to 0.5 V/Ag/AgCl in glucose-free electrolyte. Electrode polarization in the presence of 50 mM glucose was conducted in the same conditions at 1 mV s^{-1} scan rate.

3 Results and discussion

The mass fraction of polystyrene particles in the PS/CNT layer is a key parameter that was controlled during this study. As shown in Fig. 1, the PS/CNT composite can display five different composition scenarios—from pure CNT (Fig. 1a) to pure PS (Fig. 1e). The maximum volume fraction of PS is 74%, corresponding to a close-packed lattice of spheres. Cases c, d, and e all have 74 vol% occupied by PS, but the *mass fraction* of CNTs decreases from c to e, and therefore the *mass fraction* of PS continues to increase. Hence, to avoid confusion, mass fraction (or wt%) is used to describe composition. For a high-mass fraction of PS, there is insufficient CNT material to fill voids between PS spheres (Fig. 1d). Such case can lead to a CNT phase that is not inter-connected and can collapse

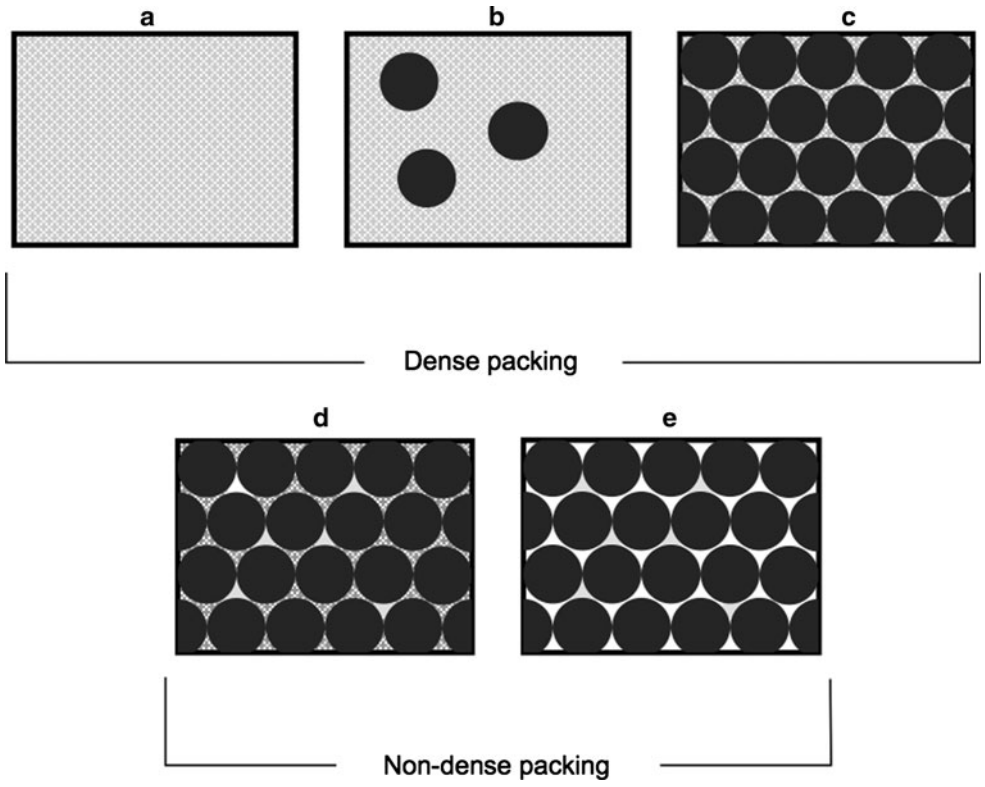

Fig. 1 Schematics of PS packing within a CNT matrix. **a** CNT matrix alone, **b** PS sparsely distributed within the CNT matrix, **c** PS close packed (74 vol%), with voids completely filled by CNT matrix, **d** PS close packed, with incomplete filling by CNT matrix, and **e** PS only

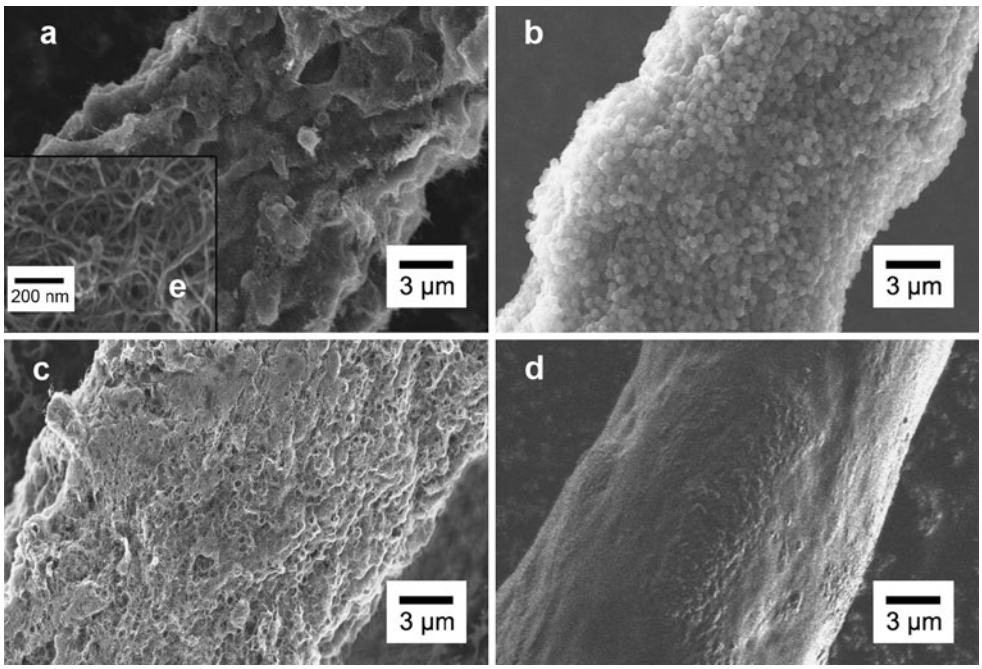

Fig. 2 Scanning electron micrographs of CFMEs at different preparation stages. **a** CNT coating (no PS particles) at 2 μg cm^{-1}, *inset* magnified view showing CNT matrix pores, **b** PS + CNT coating at PS mass fraction of 73 wt%, **c** PS + CNT coating after heat treatment. **d** Hydrogel-coated CFME at loading of 13 μg cm^{-1} and **e** *inset* showing amplified view of the CNT matrix

once the PS template is removed. For this reason, a majority of samples were made in the "dense-packing" regime, in which the CNTs were sufficient to fill the gaps. Because the densities of the CNT and PS phases are about the same, dense packing occurs for PS content of 73 wt% or less.

3.1 CFMEs under electron microscopy

The morphologies of four representative samples were observed by SEM shown in Fig. 2 and by FIB-revealed cross-section in Fig. 3. Figure 2a shows the control sample with 2 μg cm^{-1} loading of pure CNTs, displaying significant micron-scale roughness and a homogeneous nanoscale CNT matrix, consistent with literature results [21]. The cross-sectional view (Fig. 3a, inset) and side view (Fig. 4a, inset) reveal dense packing of CNTs, with average pore size of ~50 nm. This dense packing and small pore size could lead to transport limitations when the coating layer thickness is large.

A PS/CNT-modified electrode at 73 wt% PS without heat treatment was observed. The surface view (Fig. 2b) shows dense packing of particles on the surface. However, cross-section (Fig. 3b) indicates that PS particles congregated at the outer surface of the CNT layer and was not distributed uniformly in the radial direction. This may be due to the shrinkage of the CNT matrix during the evaporation of DMF solvent.

Figure 2c was obtained after heat treatment to remove 73 wt% PS particles. Although some residual PS may be present, it was not observed by SEM. Rather, the CFME surface was covered with PS-derived pores of size comparable to the original particles (500 nm). Inside the matrix, shown in Fig. 3c, macropores were distributed throughout the CNT layer, mostly in a close-packing pattern. However, few pores were apparent near the inner interface with the carbon fiber, consistent with Fig. 3b, again indicating that the PS particles did not distribute evenly through the CNT layer prior to heat treatment.

Images of the CFMEs after application of enzymatic hydrogel catalyst are shown in Figs. 2d and 3d. From previous estimations, a CNT layer of 2 μg cm^{-1} loading can contain up to 6.2 μg cm^{-1} hydrogel [21]. The hydrogel loading in Fig. 2d (13 μg cm^{-1}) almost doubled this value, yielding a surface morphology that appears much smoother than the freshly heat-treated CFMEs. The cross-sectional view in Fig. 3d shows that hydrogel successfully infiltrated and almost completely filled the pores of CNT matrix. For the purpose of microscopy, this was a dry, unhydrated gel and was expected to swell approximately twofold upon hydration, and thus completely filled the matrix [37].

3.2 Effect of heat treatment on coating morphology and surface area

Polystyrene particles were subsequently removed by heat treatment at 450 °C for 4 h. At this temperature, polystyrene gradually melts and burns away [30]. Optical microscopy was used to observe CFMEs before and after heat treatment for varying PS loadings, as shown in Fig. 4. The images were taken so that the same site at the same angle was observed to indicate the change in coating

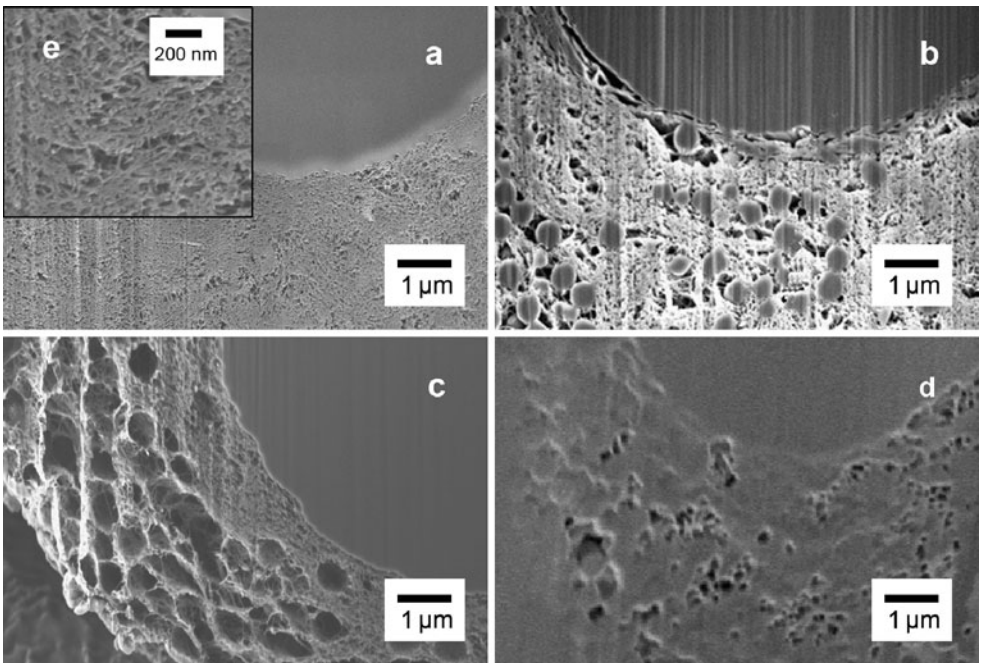

Fig. 3 Scanning electron micrographs of the focused ion beam revealed cross-sections. Samples are **a** CNT coating (no PS particles) at 2 μg cm^{-1}, *inset* magnified view showing CNT matrix pores, **b** PS + CNT coating at PS mass fraction of 73 wt%, **c** PS + CNT coating after heat treatment. **d** Hydrogel-coated CFME at loading of 13 μg cm^{-1}. *Vertical lines*, especially those in (**b**), are artifacts from the ion beam polishing

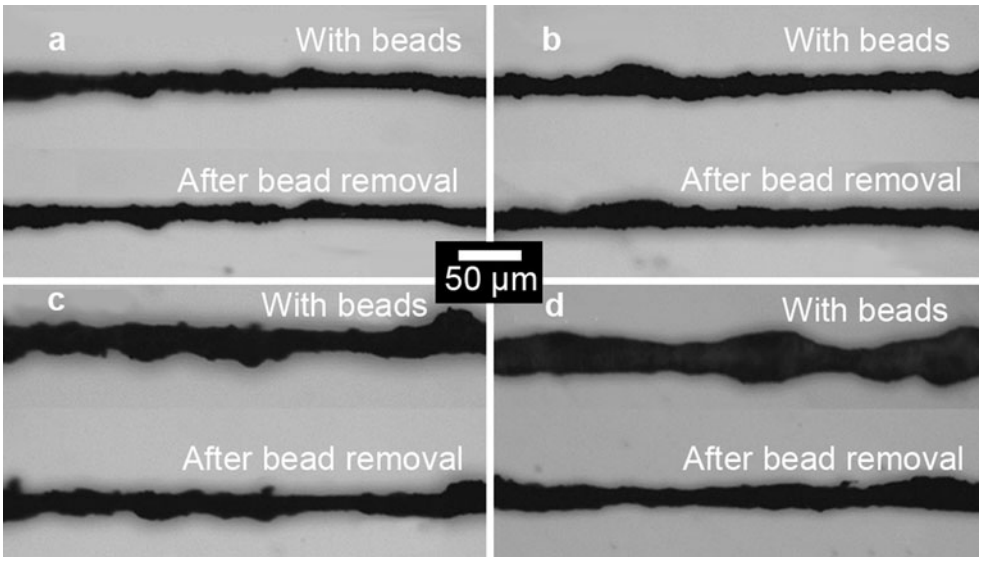

Fig. 4 Optical micrographs of CFMEs with PS particles and after particle removal with heat treatment at varying PS mass fractions. The same angle at the same spot was observed to represent morphological changes. Corresponding mass fractions are **a** CNTs alone, **b** 28 wt% PS, **c** 58 wt% PS, and **d** 73 wt% PS. CNT loading was fixed at 2 μg cm^{-1}

morphology due to heat treatment. The PS-free CFME showed no change in morphology, indicating that CNTs survived the 450 °C heat treatment.

Thickness measurements both before and after heat treatment are summarized in Fig. 5, with error bars representing sample roughness. CFME thickness with no incorporated PS beads did not change, within measurement error, due to heat treatment; the same is true for a PS loading of 29 wt%. For higher loadings of 59 and 73 wt%, a significant thickness reduction was observed. Also shown is

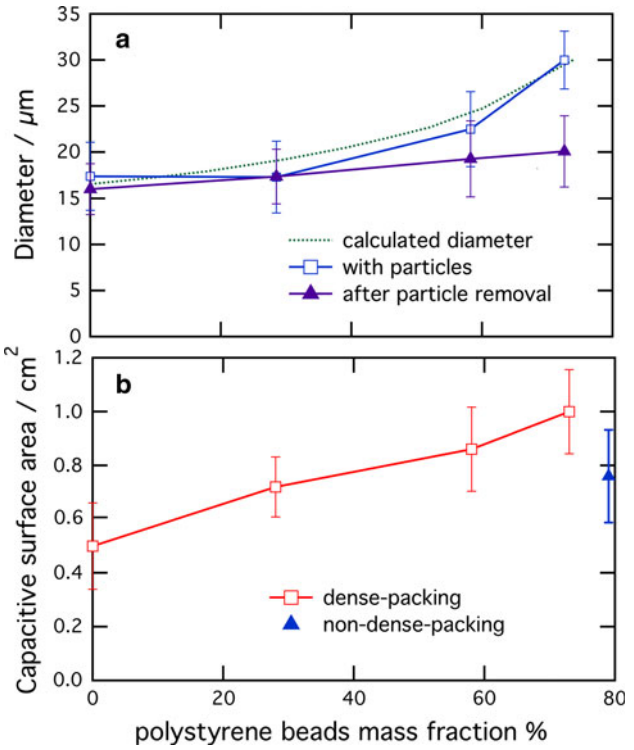

Fig. 5 Morphology trend of templated CNT-modified CFMEs. **a** PS/CNT CFME diameter before and after particle removal, estimated from the images of Fig. 4. Also shown is calculated diameter based on density estimates. **b** Capacitive surface area of PS/CNT CFMEs after bead removal with heat treatment. CNT loading mass was fixed at 2 μg cm^{-1}. Capacitance obtained by cyclic voltammetry in the 0.4–0.5 V/Ag/AgCl range in phosphate buffer solution, pH 7.0, 25 °C. Surface area was calculated from capacitance assuming a specific capacitance of 25 μF cm^{-2}

the predicted thickness prior to heat treatment, calculated using component densities and mass fractions, and assuming that the PS beads were close packed. It can be seen that the measured result and the predicted thickness match within roughness error. Even though the SEM cross-sections (Fig. 3b) showed that the PS bead distribution is not homogeneous throughout the film, the assumption of close packing appears here to be a reasonable approximation.

Some loss of CNTs is expected due to removal of the PS beads. However, the heat treatment step is not detrimental to the NT layer itself, as evidenced by the fact that, in cases of no PS template, the CNT layer thickness is maintained (Fig. 5), and the CNT surface area after heat treatment (0.5 ± 0.2 cm^2) matches that of electrodes that experienced no heat treatment (0.55 ± 0.1 cm^2) [21]. It has also previously been shown by thermogravimetric analysis that multiwall CNTs are stable up to 500 °C [38]. Moreover, the observed surface area increases with increasing PS bead loading (Fig. 5b). Thus, we rule out significant NT loss due to heat treatment.

3.3 Capacitive surface area

Due to the small scale of the electrode, electrochemical capacitance measurements were used to quantify CFME surface area, after removal of the PS template by heat treatment. Moreover, capacitance is more directly relevant to electrochemical properties, because it accounts for electronic conductivity, hydrophilicity, and infiltration of electrolyte. As summarized in Fig. 5b, increasing the mass fraction of the PS template tended to increase the capacitive surface area, such that introduction of the PS template at 74 wt% led to a doubling of the capacitive surface area compared to the PS-free samples. The PS-derived macropores therefore improved the accessibility of CNT surfaces, even though the observed CNT matrix thickness did not change. Such observations can be explained by loss of external CNTs with the removal of the PS beads during heat treatment. The remaining CNTs, although having similar thicknesses, retained higher porosity, as revealed by SEM images (Fig. 3c) and therefore higher transport efficiency.

PS mass fractions above 73 wt% led to non-dense packing (Fig. 1d, e) with insufficient CNTs to fill voids between the PS beads. One such sample was made at 79 wt% PS, as plotted in Fig. 5b. As expected, this sample showed reduced surface area comparing to dense-packing samples.

3.4 Electrochemical characterization

A biocatalyst hydrogel consisting of glucose oxidase, redox polymer, and crosslinker was coated on the PS-modified CFME as an electrochemical characterization platform. Redox polymer tests in the absence of glucose (Fig. 6a) again showed a doubling of peak current density due to the introduction of the PS template at 74 wt%. Peak separation also increases with peak height, an effect we have previously attributed to contact resistance within the electrode [21]. The observed dependence corresponds to an ohmic resistance of 24 Ω cm^2, which is lower than previous results (40 Ω cm^2) due to improvements in electrode construction.

In the presence of glucose (Fig. 6b), plateau current density at a CNT loading of 2 μg cm^{-2} with no PS template was comparable to previous results (4.1 ± 0.8 mA cm^{-2} vs. 3.5 mA cm^{-2}) within error [21]. Plateau current density was also doubled due to the introduction of 74 wt% PS, with minimal variation in half-wave potential. Performance improvement was therefore not compromised by transport limitations within the porous matrix and appeared to vary linearly with PS loading (Fig. 6 insets), suggesting that increased plateau current density is directly

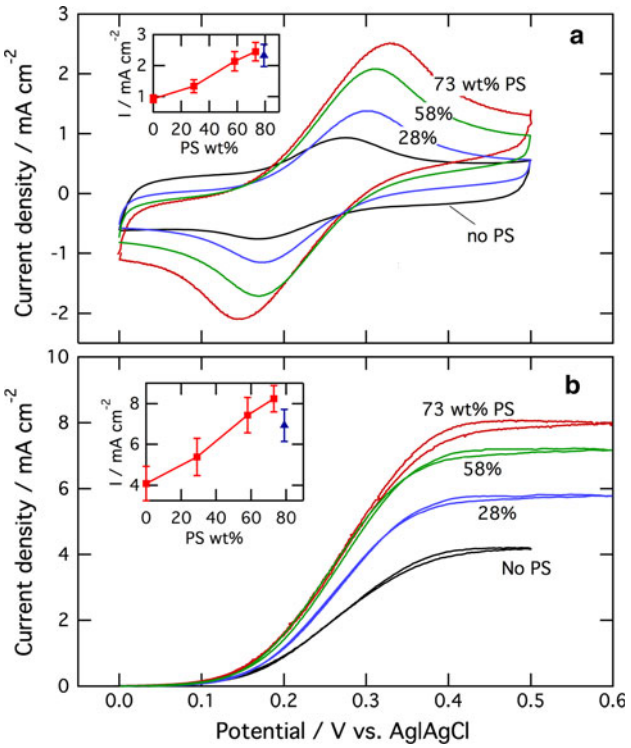

Fig. 6 Electrochemical response of glucose bioelectrodes supported on templated CNT-modified CFMEs at varying initial PS mass fractions. **a** Redox polymer voltammetry in N_2-purged PBS, pH 7.0, 37.5 °C, glucose-free, 50 mV s^{-1} scan rate. *Inset* redox polymer peak height versus PS mass fraction. **b** Glucose oxidation with 50 mM glucose, 1 mV s^{-1} scan rate. The samples were all loaded with 26 μg cm^{-1} hydrogel with 39.6 wt% GOx, 59.5 wt% redox polymer, and 0.9 wt% PEGDGE. *Inset* glucose oxidation plateau current density versus PS mass fractions. The *filled triangle* in each *inset* represents the non-dense packing case (Fig. 1d)

related to increased accessible surface area, as shown in Fig. 5b.

4 Conclusions

Introducing macropores via PS particle templating was shown to increase accessible surface area and improve performance of a biocatalyzed CFME. Introduction of the PS particle template at 74 wt%, corresponding to close packing of the PS particles with dense NT packing, led to a doubling of the capacitive surface area as compared to the untemplated samples. The templated CNT CFMEs displayed peak redox polymer and enzymatic activity properties that also doubled as compared to untemplated CNT electrodes. The hydrophilicity of the carboxylated CNT layer enabled total infiltration of biocatalytic hydrogel, as revealed by FIB−SEM. This simple procedure enables the fabrication of hierarchical multiscale porous carbon electrodes that are scalable to other applications.

References

1. Willner I, Yan Y-M, Willner B, Tel-Vered R (2009) Fuel Cells 9:7–24
2. Calabrese Barton S, Gallaway J, Atanassov P (2004) Chem Rev 104:4867–4886
3. Gregg BA, Heller A (1991) J Phys Chem 95:5970–5975
4. Nöll T, Nöll G (2011) Chem Soc Rev 40:3564–3576
5. Mano N, Mao F, Heller A (2003) J Am Chem Soc 125:6588–6594
6. Mao F, Mano N, Heller A (2003) J Am Chem Soc 125:4951–4957
7. Cooney MJ, Lau C, Windmeisser M, Liaw BY, Klotzbach T, Minteer SD (2008) J Mater Chem 18:667
8. Kim J, Jia H, Wang P (2006) Biotechnol Adv 24:296–308
9. Calabrese Barton S, Sun Y, Chandra B, White S, Hone J (2007) Electrochem Solid-State Lett 10:B96
10. Calabrese Barton S, Kim H-H, Binyamin G, Zhang Y, Heller A (2001) J Am Chem Soc 123:5802–5803
11. Calabrese Barton S, Kim H-H, Binyamin G, Zhang Y, Heller A (2001) J Phys Chem B 105:11917–11921
12. Ivnitski D, Branch B, Atanassov P, Apblett C (2006) Electrochem Commun 8:1204–1210
13. Chen T, Calabrese Barton S, Binyamin G, Gao Z, Zhang Y, Kim H-H, Heller A (2001) J Am Chem Soc 123:8630–8631
14. Mano N, Mao F, Heller A (2002) J Am Chem Soc 124:12962–12963
15. Verbrugge MW (1996) J Electrochem Soc 143:600
16. Verbrugge MW (1996) J Electrochem Soc 143:24
17. Pishko MV, Michael AC, Heller A (1991) Anal Chem 63:2268–2272
18. Gao F, Viry L, Maugey M, Poulin P, Mano N (2010) Nat Commun 1:1–7
19. Chen R-S, Huang W-H, Tong H, Wang Z-L, Cheng J-K (2003) Anal Chem 75:6341–6345
20. Zhao X, Lu X, Tze WTY, Wang P (2010) Biosens Bioelectron 25:2343–2350
21. Wen H, Nallathambi V, Chakraborty D, Calabrese Barton S (2011) Microchimica Acta 175:283–289
22. Velev OD, Kaler EW (2000) Adv Mater 12:531–534
23. Velev O, Jede T, Lobo R, Lenhoff A (1997) Nature 389:447–448
24. Iskandar F, Nandiyanto BD, Yun KM, Hogan CJ, Okuyama K, Biswas P (2007) Adv Mater 19:1408–1412
25. Holland BT, Abrams L, Stein A (1999) J Am Chem Soc 121:4308–4309
26. Jiang P, Cizeron J, Bertone JF, Colvin VL (1999) J Am Chem Soc 121:7957–7958
27. Velev O, Tessier P, Lenhoff A, Kaler E (1999) Nature 401:548
28. Flexer V, Brun N, Backov R, Mano N (2010) Energy Environ Sci 3:1302
29. Imhof A, Pine D (1997) Nature 389:948–950
30. Subramanian G, Manoharan VN, Thorne JD, Pine DJ (1999) Adv Mater 11:1261–1265
31. Vlasov YA, Deutsch M, Norris DJ (2000) Appl Phys Lett 76:1627
32. Chang H, Joo SH, Pak C (2007) J Mater Chem 17:3078
33. Chai GS, Shin IS, Yu J-S (2004) Adv Mater 16:2057–2061
34. Kinoshita K (1988) Carbon: electrochemical and physicochemical properties. Wiley, Hoboken
35. Binyamin G (1999) J Electrochem Soc 146:2965
36. Zaborsky O (1974) Biochem Biophys Res Commun 61:210–216
37. Aoki A, Rajagopalan R, Heller A (1995) J Phys Chem 99:5102–5110
38. Bom D, Andrews R, Jacques D, Anthony J, Chen B, Meier MS, Selegue JP (2002) Nano Lett 2: 615